Magnetic domain wall curvature induced by wire edge pinning

L Herrera Diez, F Ummelen, V Jeudy, G Durin, L Lopez-Diaz, R Diaz-Pardo, A Casiraghi, G Agnus, D Bouville, J Langer, et al.

Magnetic domain wall curvature induced by wire edge pinning

L. Herrera Diez,[1, a)] F. Ummelen,[2] V. Jeudy,[3] G. Durin,[4] L. Lopez-Diaz,[5] R. Diaz-Pardo,[6] A. Casiraghi,[4] G. Agnus,[7] D. Bouville,[7] J. Langer,[8] B. Ocker,[8] R. Lavrijsen,[2] H.J.M. Swagten,[2] and D. Ravelosona[1]

[1)] *Centre de Nanosciences et de Nanotechnologies, CNRS, Université Paris-Saclay, 91120 Palaiseau, France.*
[2)] *Department of Applied Physics, Eindhoven University of Technology, 5600 MB Eindhoven, the Netherlands.*
[3)] *Laboratoire de Physique des Solides, CNRS, Université Paris-Saclay, 91405 Orsay Cedex, France.*
[4)] *Istituto Nazionale di Ricerca Metrologica, Strada delle Cacce 91, 10135 Torino, Italy.*
[5)] *Departamento de Física Aplicada, Universidad de Salamanca, Plaza de la Merced s/n. 37008 Salamanca, Spain*
[6)] *Laboratoire de Physique des Solides, CNRS, Univ. Paris-Sud, Université Paris-Saclay, 91405 Orsay Cedex, France.*
[7)] *Centre de Nanosciences et de Nanotechnologies, CNRS, Univ. Paris-Sud, Université Paris-Saclay, C2N Orsay, 91405 Orsay cedex, France*
[8)] *Singulus Technology AG, Hanauer Landstrasse 103, 63796 Kahl am Main, Germany.*

In this study we report on the analysis of magnetic domain wall (DW) curvature due to magnetic field induced motion in Ta/CoFeB/MgO and Pt/Co/Pt wires with perpendicular magnetic anisotropy. In wires of 20μm and 25μm a large edge pinning potential produces the anchoring of the DWs ends to the wire edges which is evidenced as a significant curvature of the DW front as it propagates. As the driving magnetic field is increased the curvature reduces as the result of the system moving away from the creep regime of DW motion, which implies a weaker dependence of the DW dynamics on the interaction between the DW and the wire edge defects. A simple model is derived to describe the dependence of the DW curvature on the driving magnetic field and allows to extract the parameter σ_E which accounts for the strength of the edge pinning potential. The model describes well systems with both weak and strong bulk pinning potentials like Ta/CoFeB/MgO and Pt/Co/Pt, respectively. This provides a means to quantify the effect of edge pinning induced DW curvature in magnetic DW dynamics.

Keywords: magnetic micro wires, domain wall curvature, perpendicular magnetic anisotropy,

Understanding the behaviour of magnetic domain walls (DWs) when transitioning from full films into patterned structures is of great importance for developing nanodevices for DW based technologies[1]. The analysis of DW dynamics in the so called creep regime of motion[2–5], where defects play a central role, is a key aspect. In Ta/CoFeB/MgO/Ta films with perpendicular anisotropy bulk defect densities, and therefore depinning fields (H_{dep}), are relatively low[6–8]. In Pt/Co/Pt films, for example, the values of H_{dep} can be more than one order of magnitude higher[2,4,5]. Due to this low bulk pinning potential the DW dynamics can be easily controlled even in full films by artificial pinning imposed through homogeneous material engineering processes, like light ion irradiation[9–11] or pre-patterned substrates[12].

Defects generated through micro/nanostructuring can also have a great impact in pristine materials. DW velocities even in micrometer size wires have been found to experience a critical decrease below the creep law dependence at low drive which scales with the wire width[13]. This effect is also accompanied by an increase in the curvature of the DW front and has therefore been attributed to edge pinning. A deeper analysis of the DW curvature in wires is therefore needed in view of miniaturisation for technological applications.

In this study we present the analysis of the DW curvature in a series of 20μm wide Ta/CoFeB/MgO/Ta wires as a function of the magnetic field. The large edge pinning potential defines curvatures that at low drive reach the maximum radius $R = w/2$, where w is the wire width. We present a simple model that accounts for the variations in DW curvature as a function of the driving magnetic field allowing for the extraction of σ_E, a parameter that characterises the strength of the edge pinning potential. We also apply the same analysis to Pt/Co/Pt 25μm wide wires, which present a higher intrinsic bulk pinning potential. The model describes well both systems, which shows that it can be used to asses the strength of edge pinning and its influence in DW dynamics for different bulk pinning potentials.

The samples investigated are Si/SiO_2/Ta (5nm)/$Co_{20}Fe_{60}B_{20}$ (1 nm)/ MgO (2 nm)/Ta (3 nm) films deposited by magnetron sputtering and annealed at 300°C exhibiting perpendicular magnetic anisotropy. A series of 20μm wires was fabricated by photolithography and ion beam etching. The 25μm wide Pt/Co/Pt wires were fabricated by depositing a stack of Ta (4 nm)/Pt (4 nm)/Co (0.6 nm)/Pt (4 nm) by magnetron sputtering using e-beam lithography. The final wire structure was reached by conducting a lift off process. Table 1 presents the values of saturation magnetisation (M_s), effective perpendicular anisotropy constant (K_{eff}), wire width and depinning field (H_{dep}) for the two types of samples. H_{dep} corresponds to the experimentally determined transition between the creep and depinning regimes of DW motion[4,5,14].

Fig. 1 shows the Kerr microscopy images of the DW

[a)] Electronic mail: liza.herrera-diez@c2n.upsaclay.fr

Material	Width (μm)	M_s(A/m)	K_{eff} (J/m^3)	H_{dep}(mT)
CoFeB	20	8.7x10^5	3.4x10^5	9.7
Pt/Co/Pt	25	1.4x10^6	1.3x10^6	100.0

TABLE I. M_s, K_{eff}, the wire width (w) and the depinning fields H_{dep} for the Ta/CoFeB/MgO/Ta and Pt/Co/Pt wires.

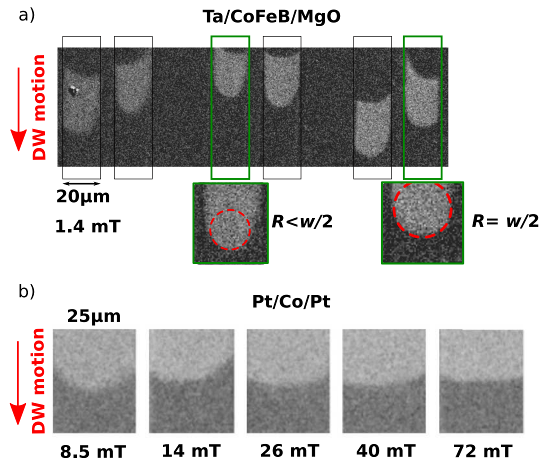

FIG. 1. (a) Kerr microscopy images of curved DWs in CoFeB wires. (b) DW curvature in a Pt/Co/Pt wire as a function of the magnetic field.

curvature for (a) the six CoFeB wires investigated, where curved DWs propagate under a magnetic field of 1.4 mT (expanding domains have a light grey color). In Fig. 1 (b) the images show the evolution of the DW curvature with increasing magnetic field in a Pt/Co/Pt wire, where as the driving field increases, the DW curvature is progressively suppressed. The difference in the applied fields at which large curvatures are observed for each film scales with the values of H_{dep}. This shows that the DW curvature is closely linked to a pinning mechanism. In order to gain more insight into this behaviour, let us first consider a DW propagating in a strip as shown in Fig. 2 (a). In this scenario the propagating DW remains straight and the Zeeman energy gain (dE_S) that the system experiences by letting the DW propagate a distance Δx is the following:

$$dE_s = -2M_s \cdot H \cdot t \cdot dA_s, \tag{1}$$

where t is the thickness of the magnetic wire and dA_s is the area swept by the DW (see Fig. 2 (a)). Let us now consider again an initial state where the DW is straight and moves by the same amount (Δx). However, the initially straight DW front can now develop a curvature of radius R as it propagates, this straight-to curved DW displacement is depicted in Fig. 2 (b). In this case the Zeeman energy gain is expressed as follows:

$$dE_c = \sigma \cdot t \cdot dL - 2M_s \cdot H \cdot t \cdot dA_c. \tag{2}$$

The gain in energy is reduced by the appearance of the first term that accounts for the variation in DW length dL

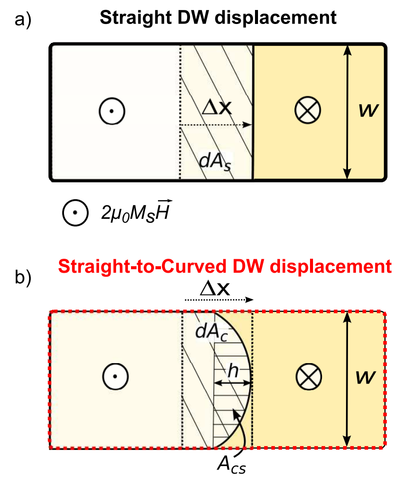

FIG. 2. Straight DW (a) and DW that transitions between a straight and a curved profile upon displacement (b).

with respect to the initial state where the DW is straight. For a straight DW its length is equal to $L = w$ while for a curved profile $L = 2R\ arcsin(\frac{w}{2R})$. This means that the additional energy cost due to the DW curvature is linked to an increase in DW length equal to $dL = 2R \cdot arcsin(\frac{w}{2R}) - w$.

The energy gain for a curved wall is also further reduced due to the smaller area swept by the DW. For a straight DW the area is $dA_S = w \cdot \Delta x$ while for the curved DW it takes the following form:

$$dA_c = w \cdot (\Delta x - h) + A_{CS}, \tag{3}$$

where h is the sagitta as indicated in Fig. 2 (b) and A_{CS} is the area of the circular sector which can be expressed as follows:

$$h = R - \sqrt{R^2 - \frac{w^2}{4}}, \tag{4}$$

$$A_{CS} = \frac{RL}{2} - \frac{w}{2} \cdot \sqrt{R^2 - \frac{w^2}{4}}. \tag{5}$$

Using these expressions we can now calculate dE_s and compare it to dE_c when, for example, the curvature radius is $R = 10\mu m$ and $w = 20\mu m$. It is not surprising to find that if no edge pinning is involved it is more energetically favourable for the DW to remain straight for all applied magnetic fields. Fig. 3 shows the result of this calculation considering the CoFeB parameters informed in Table 1, the energy gain of a straight DW (solid blue line) is always more negative than that of a curved DW (solid green line) in the whole magnetic field range.

Up to this moment no edge pinning was considered. As it is known, the curved DW scenario (Fig. 2 (b)) is a strategy to overcome edge pinning. Therefore, in order to accurately compare it to a straight DW scenario (Fig.

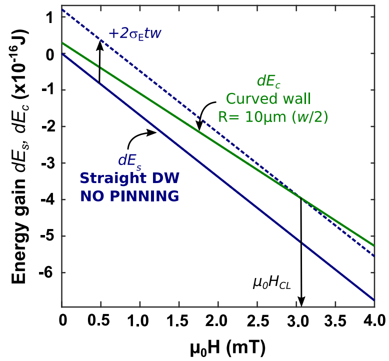

FIG. 3. Energy gain dE_s (blue line) and dE_c (green line) for straight and curved DWs as a function of the applied magnetic field in CoFeB. The straight DW without pinning increases its energy when the term $2\sigma_E \cdot t \cdot w$ is added to account for edge pinning (dotted blue line).

2 (a)), this last configuration should also include an energy cost associated with keeping the DW straight in the presence of edge pinning instead of allowing a curvature to appear. In a previous study[13] we have proposed an additional energy term to account for deviations from the creep law that are observed due to a strong edge pinning potential in CoFeB. This term includes the parameter σ_E that can be used to quantify the strength of the edge pinning and describes the effect of the pull-back that the DW experiences in a strong edge pinning potential.

In the present case, the increase in DW length observed in curved DWs due to edge pinning is taken into account by the term $\sigma \cdot t \cdot dL$. Let us assume that this energy cost due to edge pinning can find its counterpart in the hypothetic straight DW scenario as an increase in the DW energy equal to:

$$\sigma \cdot t \cdot dL = d\sigma \cdot t \cdot w. \tag{6}$$

In this context the difference in the DW energy between the initial and final states of the straight DW after a displacement Δx is proposed to be given by $d\sigma = 2\sigma_E$. This increment accounts for the effect of having two strong anchoring points of the DW at each wire side but no bending, therefore the expression for dE_s takes the form:

$$dE_s = 2\sigma_E \cdot t \cdot w - 2M_s \cdot H \cdot t \cdot dA_s. \tag{7}$$

The addition of this term shifts dE_s towards higher energies producing a crossing with dE_c as shown in Fig. 3 (dashed blue line). This crossing is the point where $dE_s = dE_c$ and defines a field limit (H_{CL}) for the existence of a DW curvature with radius R. Above this field value, it is more energetically favourable for the DW to remain straight even in the presence of edge pinning. Re-ordering the terms in $dE_s = dE_c$ allows to extract the expression for H_{CL} which has the following form:

$$H_{CL} = \frac{\sigma_E \cdot w - \sigma \cdot dL}{2M_s \cdot (w \cdot h - A_{CS})}. \tag{8}$$

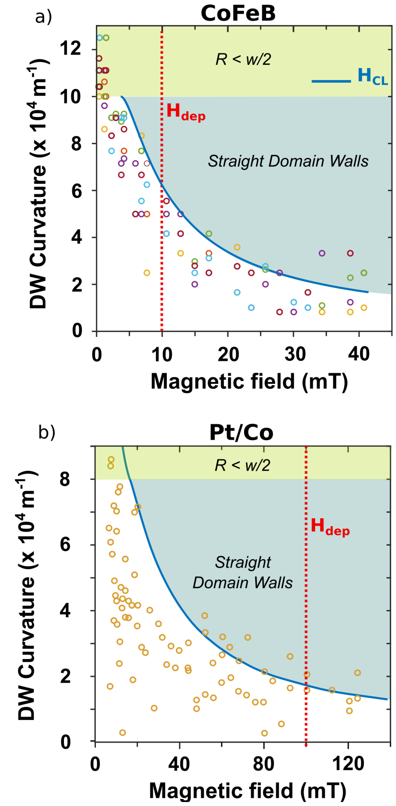

FIG. 4. Domain wall curvature as a function of magnetic field in a 20 μm wide CoFeB wire (a, different colors correspond to the different wires shown in Fig. 1) and in a 25 μm wide Pt/Co/Pt wire. The solid lines are the calculation of H_{CL}

Substituting for dL, h and A_{CS} introduces R in the equation and allows for the evaluation of the dependence of the field limit on a given range of DW curvatures ($1/R$). The experimentally observed DW curvature dependence on the applied magnetic field (symbols) together with the calculated H_{CL} (solid line) are shown in Fig. 4 (a) for CoFeB and in (b) for Pt/Co/Pt. It is worth mentioning once again that this model describes the field limit under which a given curvature can be observed, which includes the possibility of one curvature appearing at different magnetic fields below H_{CL}.

The model presented here is valid up to a maximum curvature of $2/w$, however, at low drive higher curvatures are observed for both CoFeB and Pt/Co/Pt. This occurs at magnetic fields below the value needed to depin the DW from the wire edges, even at the expense of a maximum curvature, but well above that needed to overcome pinning at the centre of the wire. In this case, it may be more energetically favourable for a DW to increase its length going from the edges to the centrer of the wire to increase the switched area. In this context, the DW front could take a more triangular shape and exhibit at the centre a curvature smaller than $w/2$. This effect can be visualized in the wires at the centre of Fig. 2 (a). The description of the curvatures above $2/w$ ($R < w/2$) at

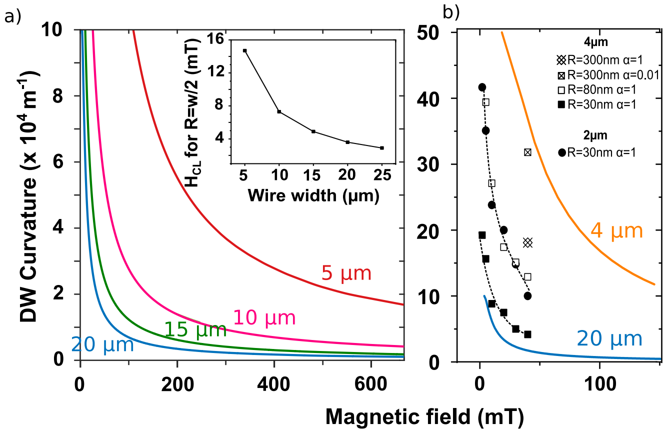

FIG. 5. (a) Calculated H_{CL} profile for σ_E=1.01x10^{-2} N/m (CoFeB) for different wire widths. H_{CL} values corresponding to R=w/2 as a function of the wire width (inset). (b) Comparison with micromagnetic simulations.

low drive is not considered in this model.

The solid curves representing H_{CL} provide a dividing line between curved and straight DWs in a magnetic field map. As mentioned, the calculation of these curves takes into account the values of K_{eff}, M_s and the width of the wire, while the value of σ_E is adjusted to model the results. The values of σ_E obtained for CoFeB and Pt/Co/Pt are 1.01x10^{-2} N/m and 6.35x10^{-2} N/m, respectively. σ_E has been introduced in a previous study as a means to quantify the strength of the edge pinning potential in the context of edge-pinning induced deviations from the creep law in CoFeB wires[13]. In this framework, it is particularly interesting to compare σ_E to the DW surface tension $\sigma = 4\sqrt{A_{ex} \cdot K_{eff}}$ where A_{ex} is the exchange stiffness constant (2.3 x 10^{-11} J/m for CoFeB and 1.6x 10^{-11} J/m for Pt/Co/Pt). The ratio σ/σ_E results in 1.1 an 0.28 for CoFeB and Pt/Co/Pt wires, respectively. It has been proposed[13] that as this ratio decreases the edge pinning potential represented by σ_E progressively dominates over the DW surface energy allowing for a DW curvature. However, when comparing values for different materials not only the differences in the intrinsic parameters but also of the bulk pinning potentials need to be taken into account. The effect of the edge pinning potential depends on its relative strength with respect to the bulk pinning potential, intimately related to the value of the depinning field H_{dep}.

The measured DW curvatures in CoFeB and Pt/Co/Pt cover a similar range going from those corresponding to R=w/2 down to low values corresponding to a large R (higher than $R = w/0.4$) for nearly straight DWs. However, the magnetic field range over which each curvature is observed is significantly different with respect to H_{dep}, which is marked by red lines in Fig. 4 (a) and (b). In CoFeB at H_{dep}, the maximum DW curvature observed experimentally and also described by the model is 6 x10^{-4} m^{-1} ($R = w/1.2$). The DW curvature is still relatively pronounced and continues to be well beyond the creep regime. Only at fields around 30 mT, three times larger than H_{dep}, do the DWs become relatively straight, showing a maximum curvature of 2 x10^{-4} m^{-1} ($R = w/0.4$). In contrast, the Pt/Co/Pt wires at H_{dep} already show relatively straight DWs with a maximum curvature below 2 x10^{-4} m^{-1}. This can be related to the large differences of about one order of magnitude found in the depinning field for the two materials. This difference also exists in full films and is due to the intrinsic bulk pinning potential that is known to be exceptionally low in CoFeB materials[2,6]. In this context, a relatively small edge pinning potential can already have a large impact on the dynamics in CoFeB while a much larger one is needed to dominate the DW dynamics in Pt/Co/Pt. Consequently, the edge pinning potential in CoFeB induces a much stronger effect than in Pt/Co/Pt, reflected here in the strong and persisting curvature of the DWs even beyond the creep regime. In contrast, in Pt/Co/Pt a significant DW curvature induced by edge pinning is only observed deep into the creep regime.

This model can also be used to extrapolate the effects of edge pinning to narrower wires. Fig. 5 (a) shows the calculated H_{CL} profiles using σ_E=1.01x10^{-2} N/m, the intrinsic parameters for CoFeB and varying the wire width. The H_{CL} values increase as the wire becomes narrower. The plot in the inset of Fig. 5 (a) shows the H_{CL} values for a DW radius of w/2 as a function of the wire width, here a dramatic increase is observed for narrow wires. This model could therefore allow for the estimation of the effects of edge pinning for a given material and a particular wire edge structure, for example linked to the fabrication process, as the wire width decreases. The estimation could be conveniently done by analysing the DW dynamics at much larger scales.

For wires widths below 5μm, it is interesting to compare this analytical model with micromagnetic simulations. Fig. 5 (b) shows the result for CoFeB wires, filled squares and circles represent the curvatures observed for w=4μm and w=2μm with an maximum edge roughness (M_{ER}) of 30nm (see supplementary information). The DW curvature follows a similar trend as the analytical model with respect to magnetic field and w. M_{ER} plays a key role, empty squares show the trend obtained for w=4μm and M_{ER}= 80nm which is reflected in a shift of the curvatures at all magnetic fields to significantly higher values. The curvature at 40mT was also evaluated in a wire with very rough edges, M_{ER}=300nm showing a further increase (crossed diamond). This is in line with the conclusions made earlier regarding the effects of the fabrication process in the DW curvature.

The curve obtained using the analytical model for w=4μm is shown in Fig. 5 (b), the curvatures are significantly larger than those obtained with micromagnetic simulations even for very large M_{ER}. It is therefore important to highlight that the micromagnetic simulations were made using the experimental values presented in Table 1 while exploring the effect of variations in the Gilbert damping parameter α. The curvatures for w=4μm in open and full squares and the crossed diamond were calculated using α =1, all showing relatively low values. For high M_{ER}, changing α from 1 (crossed diamond) to 0.01 (crossed square) increases significantly the curvature, as seen at 40mT. CoFeB is known to have low values of α in the 0.015 range[15], therefore lower α values not only give curvatures closer to the analytical model but are also more compatible with experimental values.

In contrast, for low M_{ER} the effect of varying α is not a dominant feature. This bring the attention to the crucial role of disorder in the DW dynamics in CoFeB. In the present study, perfect wires are simulated, while studies in the literature show that adding a granular structure and an anisotropy distribution to simulate disorder can have a large impact in the DW dynamics. In this context, additional energy dissipation channels appear in the system which could also affect the response to a change in the value of α[11]. A detailed micromagnetic study would be needed to fully characterise these effects.

Micromagnetic simulations have also been performed for w=250nm and w=500nm, where the analytical model finds its limit of validity since it is based on the one dimensional(1D) model of DW motion. A dimensionality change may occur from a 2D to a 1D medium for very narrow wires[16] and edge effects can rule over creep dynamics[17] limiting the use of a 1D based model. For w=500nm, M_{ER}=30nm and α =0.015 the internal structure of the DW presents a large number of Bloch lines and an irregular DW front, showing no curvature for either 10mT nor 20mT. A similar behavior is observed for w=250nm (see supplementary information). This confirms the presence of a more complex dynamics at this scale going beyond the 1D model and calls for a more careful theoretical analysis.

In conclusion, we present a simple model to describe the dependence of the DW curvature on the applied magnetic fields in wires with an edge pinning potential. This model allows for the estimation of the magnetic field limit up to which a given DW curvature can be observed and it has been applied to two key spintronics materials with low and high bulk pinning potentials, CoFeB and Pt/Co/Pt. The analysis of the DW curvature also allows for the extraction of the parameter σ_E that can be used to compare edge pinning potentials in different devices. The relative strength of the edge pinning potential with respect to the surface tension of the DW (σ/σ_E) together with the differences between the edge and bulk pinning potentials in each material are the key aspects involved in the description of the DW curvature. It has also been shown that this model can be used to extrapolate the effects of edge pinning observed in relatively large wires to smaller dimensions and has a good correspondence with results obtained from micromagnetic simulations. Therefore, this model can be of considerable interest for the understanding and the quantification of the effects of edge pinning in patterned magnetic structures.

SUPPLEMENTARY MATERIAL

Information about micromagnetic simulations.

ACKNOWLEDGMENTS

We gratefully acknowledge financial support from the European Union FP7 and H2020 Programs (MSCA ITN grants No. 608031 and No. 860060), from the French National Research Agency (project ELECSPIN), and Ministerio de Economia y Competitividad of the Spanish Government (project MAT201787072C41P). The authors thank G. van der Jagt for useful comments.

DATA AVAILABILITY STATEMENT

The data that support the findings of this study are available from the corresponding author upon reasonable request.

[1] S. S. P. Parkin, M. Hayashi and L. Thomas, *Science* **320**, 190194 (2008).

[2] P. J. Metaxas, J. P. Jamet, A. Mougin, M. Cormier, J. Ferre, V. Baltz, B. Rodmacq, B. Dieny, R. L. Stamps. *Phys. Rev. Lett.* **99**, 217208 (2007).

[3] P. Metaxas. *Solid State Physics* Vol. **62**, Ch. 2, Academic Press Inc.(2011).

[4] S. Lemerle, J. Ferré, C. Chappert, V. Mathet, T. Giamarchi, P. Le Doussal. *Phys. Rev. Lett.* **80**, 849 (1998).

[5] V. Jeudy, A. Mougin, S. Bustingorry, W. Savero Torres, J. Gorchon, A. B. Kolton, A. Lematre, and J.-P. Jamet. *Phys. Rev. Lett.* **117**, 057201 (2016).

[6] C. Burrowes, N. Vernier, J.-P. Adam, L. Herrera Diez, K. Garcia, I. Barisic, G. Agnus, S. Eimer, Joo-Von Kim, T. Devolder, A. Lamperti, R. Mantovan, B. Ockert, E. E Fullerton, D. Ravelosona, *Appl. Phys. Lett.* **103**, 182401 (2013).

[7] R. Lavrijsen, G. Malinowski, J.H. Franken, J.T. Kohlhepp, H.J.M. Swagten, B. Koopmans, M. Czapkiewicz, and T. Stobiecki, *Appl. Phys. Lett.* **96**, 022501 (2010).

[8] J.-P. Tetienne, T. Hingant, J.-V. Kim, L. Herrera Diez, J.-P. Adam, K. Garcia, J.-F. Roch, S. Rohart, A. Thiaville, D. Ravelosona and V. Jacques, *Science* **344**, 1366 (2014).

[9] J. Fassbender, D. Ravelosona, Y. Samson. *J. Phys. D: Appl. Phys.* **37** R179196 (2004).

[10] L. Herrera Diez, F. García-Sánchez, J.-P. Adam, T. Devolder, S. Eimer, M. S. El Hadri, A. Lamperti, R. Mantovan, B. Ocker, and D. Ravelosona, *Appl. Phys. Lett.* **107**, 032401 (2015).

[11] L. Herrera Diez, M. Voto, A. Casiraghi, M. Belmeguenai, Y. Roussign, G. Durin, A. Lamperti, R. Mantovan, V. Sluka, V. Jeudy, Y. T. Liu, A. Stashkevich, S. M. Chrif, J. Langer, B. Ocker, L. Lopez-Diaz, and D. Ravelosona *Phys. Rev. B* **99**, 054431 (2019).

[12] A. Digiacomo, R. Mantovan, N. Vernier, T. Devolder, K. Garcia, G. Tallarida, M. Fanciulli, A. Lamperti, B. Ocker, L. Baldi, M. Mariani, and D. Ravelosona, *Phys. Rev. Applied* **10**, 064053 (2018).

[13] L. Herrera Diez, V. Jeudy, G. Durin, A. Casiraghi, Y.T. Liu, M. Voto, G. Agnus, D. Bouville, L. Vila, J. Langer, B. Ocker, L. Lopez-Diaz, and D. Ravelosona, *Phys. Rev. B* **98**, (2018).

[14] R. Diaz Pardo, W. Savero Torres, A. B. Kolton, S. Bustingorry, and V. Jeudy. Phys. Rev. B 95, 184434 (2017).

[15] C. Burrowes, N. Vernier, J.-P. Adam, L. Herrera Diez, K. Garcia, I. Barisic, G. Agnus, S. Eimer, J.-V. Kim, T. Devolder, A. Lamperti, R. Mantovan, B. Ockert, E.E. Fullerton, and D. Ravelosona, Appl. Phys. Lett. 103, 182401 (2013).

[16] K.-J. Kim, J.-C. Lee, S.-M. Ahn, K.-S. Lee, C.-W. Lee, Y.J. Cho, S. Seo, K.-H. Shin, S.-B. Choe, and H.-W. Lee, Nature 458, 740 (2009).

[17] X. Zhang, N. Vernier, W. Zhao, L. Vila, and D. Ravelosona, AIP Advances 8, 056307 (2017).